JOURNAL OF MATERIALS SCIENCE: MATERIALS IN MEDICINE 15 (2004) 705–710

The effect of hot pressing on the physical properties of glass reinforced hydroxyapatite

G. GEORGIOU, J. C. KNOWLES*
Division of Biomaterials and Tissue Engineering, Eastman Dental Institute, University College London, 256 Gray's Inn Road, London, WC1X 8LD, UK
E-mail: j.knowles@eastman.ucl.ac.uk

J. E. BARRALET
Biomaterials Unit, School of Dentistry, The University of Birmingham, St Chad's Queensway, Birmingham, B4 6NN, UK

Y. M. KONG, H. E. KIM
School of Material Science and Engineering, Seoul National University, Seoul 151–742, South Korea

Hydroxyapatite (HA), being of physiological importance, can be developed synthetically for implant application. A number of avenues have been explored in order to improve the physical and biological properties of a variety of hydroxyapatite composites. However, the fact remains, hydroxyapatite lacks the mechanical properties needed to sustain high loads. This study investigates the advantages of hot pressing on the physical properties of HA and glass reinforced HA (GR-HA). The results show a significant enhancement in the mechanical properties of GR-HA composites compared to HA e.g. flexural bending strength values were given at 91.75 and 88.87 M Nm^{-2} for GR-HA (CP15F) and GR-HA (CP20F) respectively, compared to 78.9 M Nm^{-2} for HA. The results for other properties such as elastic modulus, fracture toughness, Vicker's hardness, density and porosity also demonstrate the benefit of adding phosphate based glasses as a sintering aid. This is supported by XRD analysis, highlighting the presence of a secondary phase (β-TCP) in GR-HA systems and the positive effect it has on the physical properties. It must be brought to attention that densification of hot pressed HA and GR-HA composites is reached at a lower temperature compared to a previous study on the same materials that have undergone pressureless sintering.

Introduction

Hydroxyapatite (HA) has generated a great deal of interest over recent years as a surgical implant material [1]. This is attributed to its bioactive nature which stems from the chemical similarity it has with the inorganic phase of natural bone [2–6]. Biologically, HA can serve as a means by which tissue, such as bone, can regenerate, and can be developed in various forms to serve this purpose either as a scaffold [7], coating [8] or as a monolithic block [9]. However, mechanically, HA is limited due to its low load bearing capacity [1].

Studies have shown that the introduction of phosphate based glasses as a sintering aid is known to reinforce HA mechanically [6]. Furthermore, phosphate glasses are known to facilitate the decomposition of the HA phase to β-tricalcium phosphate (β-TCP) and can also lead to further inversion of the β-TCP phase to α-TCP [3–6]. These phase changes can be brought about by ionic substitutions between the glass and HA that occur during liquid phase sintering and the extent of substitution can depend on the chemical nature of the glass [3, 6]. Some glasses may contain ions such as Na^+ or Mg^{2+}, which could also be responsible for structural changes in the HA lattice during the sintering process.

In addition to the additives (phosphate glasses) used to improve physical properties, one must consider the various sintering routes that can be employed. Previous studies have demonstrated the effect of uniaxial pressureless sintering on the biaxial flexure strength and other physical properties of HA and glass reinforced HA (GR-HA) [10, 11]. An alternative sintering route known as hot pressing involves simultaneous pressing and firing carried out under high vacuum. The physical properties of materials that are hot pressed are generally expected to be greater than those that are sintered under no pressure. The hot pressing method is considered to accelerate the sintering process by improving the packing and interparticulate contact and as a result enhance the density and greatly reduce the porosity of the material.

*Author to whom all correspondence should be addressed.

TABLE I Glass composition used and precursor amounts

	Amount of constituent in glass (mol%)			Amount of precursor added (g)		
Glass code	CaO	P_2O_5	CaF_2	$CaHPO_4$	P_2O_5	CaF_2
CP15F	21.25	63.75	15	14.44	15.09	2.928
CP20F	16.25	63.75	20	11.05	16.86	3.904

The purpose of this study was to characterise the physical properties of hot pressed HA and GR-HA materials.

Materials and methods

Phosphate glass preparation

Two glass compositions were selected for incorporation into HA. The two ternary glasses were formulated from the same three components; P_2O_5, $CaHPO_4$ and CaF_2. The main network forming component that was introduced was P_2O_5, however, the difference in composition between both glasses was the amount of CaF_2 and CaO added (Table I). The starting reagents required to make the selected glass where mixed thoroughly and placed in a platinum crucible, melted between 1000 and 1100 °C for 1 h, and then poured onto a steel plate and allowed to cool. The resulting glass was then ground to a fine powder using a ball and agate grinder.

Preparation of HA and GR-HA

Milling of HA

HA (200 g) and methanol (300 ml) were placed into a porcelain mill pot and the mixture was then wet milled for 24 h.

Milling of GR-HA

The glass (5 g) was placed into a porcelain mill pot (Pascall Engineering Co. Ltd, UK) and milled dry for 24 h. HA (195 g) (supplied by Plasma Biotal Ltd, UK) was then added to the mill pot to make a 2.5% glass weight addition. Methanol GPR grade (BDH Laboratory Supplies, UK) (300 ml) was also added and the mixture was then wet milled for a further 24 h.

The resulting slip that was obtained from milling was then dried at 70 °C and the dry powder was then sieved to give a particle size of less than 75 μm using a vibratory sieve shaker (Fritsch, Germany) through Endecotts sieves (supplied by Christisons, Newcastle, UK) with aperture sizes of 1 mm, 200, 150, 100 and 75 μm.

Hot pressing

The sieved HA/GR-HA powder (25 g) was poured into a graphite sheet lined carbon mould and the powder was compacted, initially, to ≈ 1 ton using a manual hydraulic pump. The mould was constructed to form $40 \times 40\,mm^2$ ceramic blocks. The graphite mould was then placed into a vacuum hot press chamber (JungMin High Vac. Co., Korea). The chamber was then pumped with a mechanical rotary pump to between 200 and 300 mTorr. The rotary vacuum pump was turned off and the diffusion pump was then turned on and the chamber was pumped to obtain a vacuum level of about 30–60 mTorr. In order to obtain this level of vacuum and to ensure that only an inert gas is present during degassing, the chamber was purged several times with Ar gas. Once this vacuum level was reached, the chamber was heated at a rate of $10\,°C\,min^{-1}$ to the sintering temperature. Once the temperature reached 600–650 °C, Ar gas was allowed to flow through the chamber and then the vacuum was turned off. During the following stage, the vacuum slowly rose back to atmosphere through a combination of some degassing and the continual purging with Ar. From this point, the powder was compacted stepwise using a hydraulic oil press until it reached the sintering temperature (1100 °C) where full load (3500 kg) was applied. The powder was compacted and sintered at this temperature for 1 h. After heating at the required temperature the hydraulic pump was then turned off, the inlet and outlet gas valves were shut, and the furnace was allowed to cool. The resulting hot pressed blocks that were produced were $40 \times 40 \times \sim 5$ mm in dimension.

Specimen block preparation

The blocks were cut using a diamond saw (Daisan machine Co., Korea) to $40 \times 5 \times 4$ mm bars suitable for four point bending tests. They were then ground to a thickness of 3 mm to $40 \times 4 \times 3$ mm. The tensile test surface of the specimen blocks were polished to 1 μm and the edges of that surface were bevelled to eliminate edge cracks/flaws.

Density determination

The density measurements were determined using the saturated weight of the sample. This measures the amount of water that is saturated by the sample and takes into consideration the porosity of the sample. This can be calculated by the following equation:

$$\text{Real density} = \frac{\text{dry weight}}{(\text{saturated weight} - \text{suspended weight})} \times \rho_w$$

X-ray diffraction

Tested samples were ground to a fine powder, placed in a specimen holder and then analysed on a Philips PW1070 diffractometer with Ni filtered CuK_α radiation ($K_{\alpha1} = 1.5406$ Å, $K_{\alpha2} = 1.5444$ Å) at 40 kV and 30 mA. The data were collected with a scintillation counter between $10 < 2\theta < 100°$ with a step size of 0.02° and count time of 12 s using flat plate geometry.

Structure refinement

The structure refinement was carried out using general structure analysis software (GSAS, Los Alamos National Laboratory). A standard model for each of the three phases was used for the refinement of the samples and they were determined from the Daresbury Crystal Structure Database. The HA model was based on the single crystal structure determination with $P6_3/m$ [12] space group and the β-TCP second phase was based on the R3CH model [13].

The software calculates the phase weight percentage (P) and the theoretical density(ρ) (assuming no porosity) of each phase present in the specimen. The calculation for these numbers does not include any error determination. From these, the overall theoretical density of the sample can be determined:

$$(P_{HA} \times \rho_{HA}) + (P_{\beta-TCP} \times \rho_{\beta-TCP}) + (P_{\alpha-TCP} \times \rho_{\alpha-TCP}) = \text{overall theoretical density}$$

From the data for the measured density and the overall theoretical density, the porosity is calculated using

$$[1 - (\text{Recorded density}/\text{Theoretical density})] \times 100(\%)$$

This again does not have an associated error with it.

Four point bend test

The specimen bars that were prepared by hot pressing were mechanically tested using the four point bending test (Tesilon Toyo Baldwin, A&D Co. Ltd, Japan) at a crosshead speed of 1 mm min^{-1} to failure. The bars were supported by two support bars that were 30 mm apart. The load span consisted of two loading bars that were 10 mm apart. The flexural bend strength was determined by the following equation:

$$\sigma_{b4} = \frac{3P(L-I)}{2Wt^2}$$

where σ_{b4} is the flexural strength in four point bending, P the load (N), L the outer span, I the inner span, W the width of specimen and t the thickness of specimen.

Elastic modulus

The modulus of elasticity for the hot pressed specimens was determined using the ultrasound method. This measures the time it takes for an ultrasound wave to travel the thickness of the sample, in both longitudinal and transverse directions. This value is converted in to velocity. Together with the density of the sample and Poisson's ratio the value for elasticity can be calculated:

$$V_l = \frac{2d}{T_l}, \quad V_t = \frac{2d}{T_t},$$

$$\text{Poisson's ratio } \nu = \frac{1 - 2(V_t/V_l)^2}{2 - 2(V_t/V_l)^2}$$

$$\text{Elastic modulus } (E) = \frac{V_l^2 \rho(1+\nu)(1-2\nu)}{(1-\nu)}$$

where V_l and V_t are the longitudinal and transverse velocities respectively, T_l and T_t are the longitudinal and transverse time respectively, d the thickness of the sample and ρ the density of the sample.

Fracture toughness and hardness

The fracture toughness and hardness values for the hot pressed specimen bars were determined by the indentation method. Indentations were carried out using a Vickers microhardness indentor (Mitutoyo). The dimensions of the cracks that were induced by an indentation load and also the dimensions of the indentations were used to calculate the fracture toughness and hardness with respect to indentation alone

$$Kc = 0.016 \left[\frac{E}{H}\right]^{1/2} \frac{P}{C^{3/2}} \quad H_v = \frac{1.8544 P_H}{(2a)^2}$$

where, E is the elastic modulus, H_v the hardness, P the indentation load to induce a crack, C the crack length: half the average of the two cracks, P_H the indentation load and a the half the average of the two indent diagonals.

Results

The mean flexural bend strength data (Fig. 1) gave values of 78.90, 91.75 and 88.87 M Nm^{-2} for HA, GR-HA (CP15F) and GR-HA (CP20F) respectively. As is expected the mean values show an increase in the mean flexural strength for the GR-HA specimens, however, there is a substantial overlap in the standard deviation between the three sets of data.

The elastic modulus data (Fig. 2) also shows an increase in the mean values for the GR-HA composites compared with HA. These were recorded at 105.91, 112.80 and 117.87 G Nm^{-2} for HA, GR-HA (CP15F) and GR-HA (CP20F) respectively.

The fracture toughness values (Fig. 3) for these materials showed an increase in the mean values for the GR-HA materials compared with HA, however, the GR-HA systems displayed no significant difference between the two sets of data. The mean values were recorded at 0.98, 1.1997 and 1.232 M Nm$^{-3/2}$ for HA, GR-HA (CP15F) and GR-HA (CP20F) respectively. The results given for the hardness (Fig. 4) showed a significant overlap in data between GR-HA (CP15F) and GR-HA (CP20F), however, the results given for HA

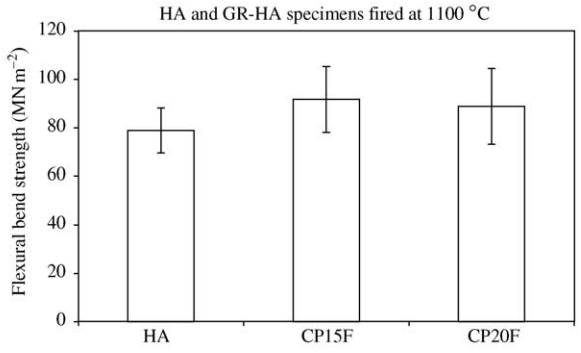

Figure 1 Flexural bend strength.

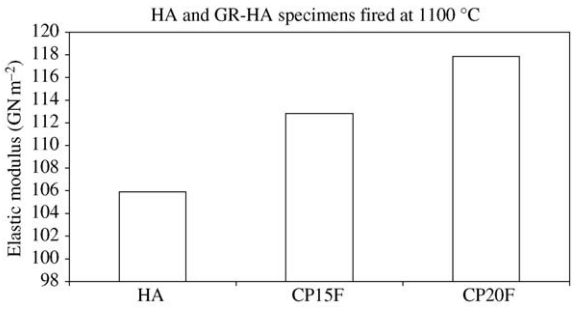

Figure 2 Elastic modulus.

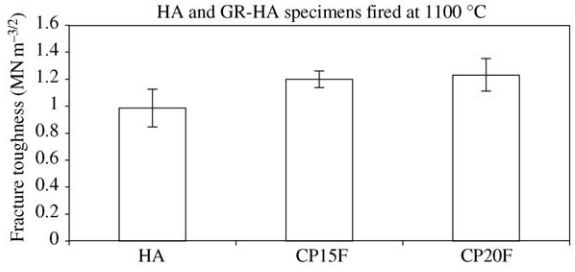

Figure 3 Fracture toughness.

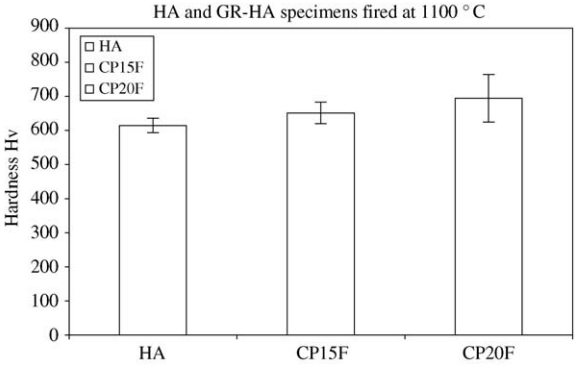

Figure 4 Hardness.

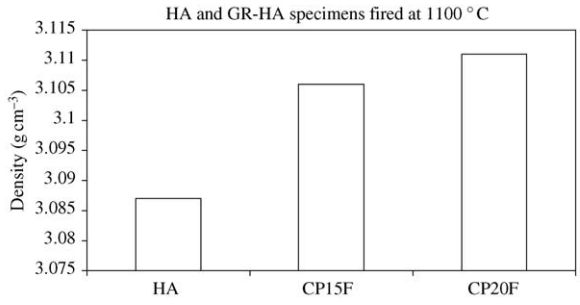

Figure 5 Density.

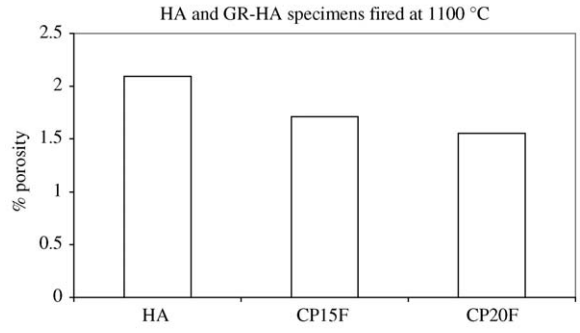

Figure 6 Porosity.

were significantly lower when compared with both GR-HA composites. The mean values that were recorded were given at 613.8, 650.4 and 693 H_v for HA, GR-HA (CP15F) and GR-HA (CP20F) respectively.

It has been reported that the addition of phosphate glasses to HA serves to enhance densification and minimise porosity of HA through liquid phase sintering and this is supported by the data given in Figs. 5 and 6.

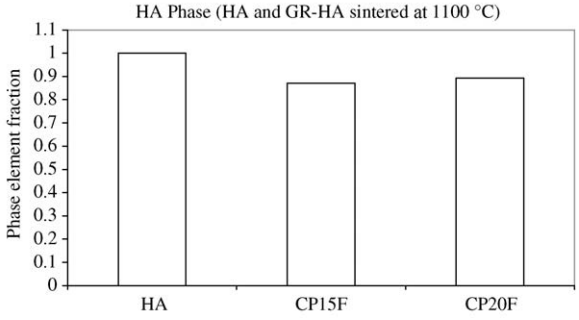

Figure 7 Phase element fraction (HA phase).

The increase in densification when comparing HA and GR-HA values was between 6 and 8%. Furthermore, the densification data correlates with the porosity data. As GR-HA materials undergo liquid phase sintering the interparticulate contact is greater, which in effect, accelerates grain growth (Figs. 9–11) and thus facilitates the elimination of pores which are present in grain centres and along grain boundaries. Examination of the micrographs shows that while the hot pressed HA (Fig. 9) has some porosity, for the two composites (Figs. 10 and 11), porosity is virtually eliminated. There is evidence for grain growth in the composites, however, this is not considered to be excessive and clearly the grain size effect is offset by the virtually 100% density achieved.

X-ray diffraction analysis shows a typical trend in the behaviour of GR-HA materials. At 1100 °C, the GR-HA materials display a drop in the fraction of the HA constituent phase (Fig. 7) coinciding with an increase in the β-TCP phase (Fig. 8). This is clearly indicative of HA decomposition to a secondary phase of β-TCP. The β-TCP phase constituted 12.9 and 10.7% of the GR-HA (CP15F) and GR-HA (CP20F) composite materials respectively.

5. Discussion

The increase in the mean value for flexural bend strength (Fig. 1) may be explained by the fact that as the GR-HA's are fired at the sintering temperature, the HA phase undergoes decomposition to the secondary β-TCP phase (Figs. 7 and 8). Phase transformations to secondary phases of greater unit cell volume such as β-TCP usually bring about residual stress thus providing greater strength to the material. The mean strength values have been known to vary from one GR-HA composite to another

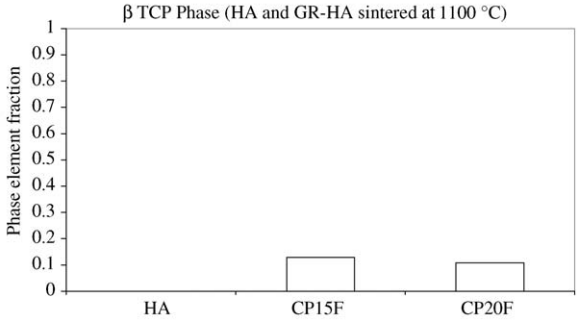

Figure 8 Phase element fraction (β-TCP phase).

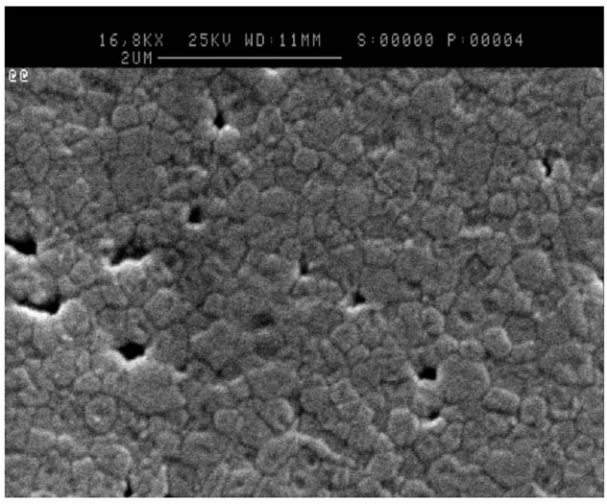

Figure 9 SEM micrograph of HA hot pressed at 1100 °C.

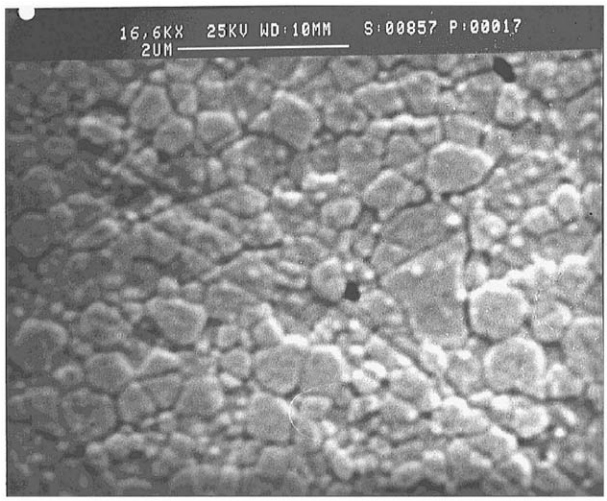

Figure 10 SEM micrograph of GR-HA (CP15F) hot pressed at 1100 °C.

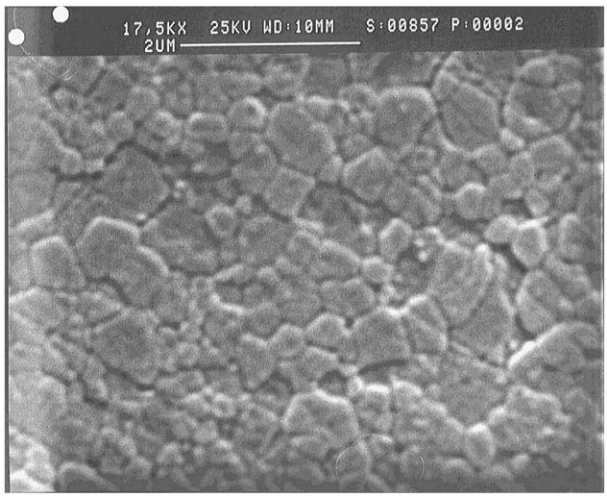

Figure 11 SEM micrograph of GR-HA (CP20F) hot pressed at 1100 °C.

and this depends upon the physical properties of the glass composite. The physical properties are governed by the type of components present in the glass and the amount of each component. This may explain the differences in strength values measured for the GR-HA's. Studies have shown that the flexural strength of the same composite materials developed via pressureless sintering is significantly lower [14]. These were recorded in the range between 30.327 and 47.35 MNm^{-2}. These differences can be explained by the fact that as these materials are simultaneously pressed and fired to temperature, densification is reached more quickly due to greater compaction/interparticulate contact and as a result greatly reduces porosity and subsequently provides greater strength.

The elastic modulus results that are presented in Fig. 2 also show enhanced values for the GR-HA composites compared with HA. The enhanced stiffness values for the GR-HA composites are mainly attributed to the behaviour of the glass during sintering. The viscous nature of the glass allows diffusion of ions from the glassy phase to the HA matrix, allowing ion exchange such as F^- for OH^- in the hydroxyl channels. As a result, greater chemical bonding interactions occur between ions such as F^- with Ca^{2+} in the hydroxyl channels due to the electronegativity of F^-, and consequently, serves to reduce inter-atomic spacing. In addition, the presence of secondary phases such as β-TCP may serve to increase the flexural modulus of a GR-HA system. The modulus of a material consisting of more than one phase can be approximated to be the sum of the moduli of each constituent phase. No standard deviation values were given in this case since the ultrasound method employed only requires one specimen from each material/composite for analysis.

The fracture toughness (Fig. 3) data given also exhibit higher mean values for the GR-HA composites compared with HA. The presence of pores within materials can be considered to behave like flaws and therefore have an influence on the fracture properties. An increase in densification (Fig. 5) and the consequent reduction in porosity (Fig. 6) for the GR-HA systems limit the effect of flaws. In addition, the presence of two phases which have different fracture properties limits crack propagation to the grain boundary interface between two different phases. This effect is brought about by the ability of the tougher phase to absorb the stress. Hence, the tougher fracture properties of the β-TCP phase contributes to the increase in fracture toughness of GR-HA composites.

The increase in the mean hardness values (Fig. 4) for the GR-HA composites can be attributed to increased densification and reduction in porosity compared with HA. However, the aforementioned properties regarding materials consisting of more than one phase is also considered in this case, as β-TCP is known to have greater hardness properties than HA. SEM clearly supports the calculations made for the porosity and density and the difference in porosity levels between the HA and the GR-HA composites can be seen (Figs. 9–11). SEM also highlights that the addition of the glass enhances the sintering mechanism, with two changes occurring: a significant reduction in porosity and a

concurrent increase in grain size. However, the grain size increase in the GR-HA composites was not excessive and is offset by the reduction in porosity.

6. Conclusion

The addition of phosphate glasses during the sintering process serves to enhance the mechanical properties of HA as the results have shown. The method of incorporating glasses as a sintering additive to HA is widely known, and it is shown to increase densification and minimise porosity. This effect can be attributed to liquid phase of the glass during sintering. However, an alternative method of sintering known as hot pressing can further accelerate the sintering process, which as a result allows GR-HA materials to reach densification at lower temperatures and further reduce porosity relative to pressureless sintered materials [14].

The presence of β-TCP secondary phase in hot pressed GR-HA composites correlate with the increase in mechanical properties, much like they do for the pressureless sintered GR-HA composites. Furthermore, the SEM micrographs showed an increase in grain size for the GR-HA composites compared with HA. The increase in the rate of grain growth for GR-HA composites has shown to reduce greatly the number of pores and therefore improve the fracture properties.

References

1. M. MARCACCI, E. KON, S. ZAFFAGNINI, R. GIARDINO, M. ROCCA, A. CORSI, A. BENVENUTI, P. BIANCO, R. QUARTO, I. MARTIN, A. MURAGLIA and R. CANCEDDA, *Cal. Tissue Int.* **64** (1999) 83.
2. J. C. KNOWLES, S. CALLCUT and G. GEORGIOU, *Biomaterials* **21** (2000) 1387.
3. J. D. SANTOS, P. L. SILVA, J. C. KNOWLES, S. TALAL and F. J. MONTEIRO, *J. Mater. Sci. Mater. Med.* **7** (1996) 187.
4. J. C. KNOWLES, S. TALAL and J. D. SANTOS, *Biomaterials* **17** (1996) 1437.
5. J. C. KNOWLES, *Br. Ceramic Trans.* **93** (1994) 100.
6. J. C. KNOWLES and W. BONFIELD, *J. Biomed. Mater. Res.* **27** (1993) 1591.
7. S. CALLCUT and J. C. KNOWLES, *J. Mater. Sci. Mater. Med.* **13** (2002) 485.
8. J. C. KNOWLES, K. GROSS, C. C. BERNDT and W. BONFIELD, *Biomaterials* **17** (1996) 639.
9. H. AKAO, H. AOKI and K. KATO, *J. Mater. Sci. Mater. Med.* **16** (1981) 809.
10. G. GEORGIOU and J. C. KNOWLES, *Biomaterials* **22** (2001) 2811.
11. D. W. RICHERSON, in ''Modern Ceramic Engineering'' (Marcel Dekker, 1992).
12. M. I. KAY, R. A. YOUNG and A. S. POSNER, *Nature* **204** (1964) 1050.
13. L. W. SCHROEDER, B. DICKENS and W. E. BROWN, *J. Solid State Chem.* **22** (1977) 253.
14. G. GEORGIOU, PhD Thesis, University of London (2002).

Received 14 July
and accepted 28 October 2003